Dimension Characteristics and Precipitation Efficiency of Cumulonimbus Clouds in the Region Far South from the Mei-Yu Front over the Eastern Asian Continent

YUKARI SHUSSE* AND KAZUHISA TSUBOKI

Hydrospheric Atmospheric Research Center, Nagoya University, Nagoya, Japan

(Manuscript received 22 February 2005, in final form 26 August 2005)

ABSTRACT

Dimension characteristics in precipitation properties of cumulonimbus clouds are basic parameters in understanding the vertical transport of water vapor in the atmosphere. In this study, the dimension characteristics and precipitation efficiency of cumulonimbus clouds observed in the Global Energy and Water Cycle Experiment (GEWEX) Asian Monsoon Experiment (GAME) Huaihe River Basin Experiment (HUBEX) are studied using data from X-band Doppler radars and upper-air soundings. The maximum echo area (EA_{max}) of the cumulonimbus clouds ranged from 0.5 to 470 km^2, and the maximum echo top (ET_{max}) ranged from 2 to 19 km. The total number of cells (TNC) within the cumulonimbus clouds over their lifetime was from 1 to 25.

The ET_{max}, TNC, area time integral (ATI), and total rainfall amount (R_{tot}) strongly correlate with the EA_{max} of the cumulonimbus clouds. The cell-averaged ATI (ATI_{cell} = ATI/TNC), maximum rainfall intensity (RI_{max}), and cell-averaged rainfall amount ($R_{cell} = R_{tot}$/TNC) increase when the EA_{max} is smaller than 100 km^2. On the other hand, they are almost constant when the EA_{max} is larger than 100 km^2. The rain productivity of small clouds (<100 km^2 in EA_{max}) increases not only by the increase of the TNC but also by the intensification of cells, while that of large cumulonimbus clouds (>100 km^2 in EA_{max}) increases by the increase of the TNC rather than by the intensification of cells.

In the present study, precipitation efficiency (ε_p) is defined as the ratio of the total rainfall amount (R_{tot}) to the total water vapor amount ingested into the cloud through the cloud base (V_{tot}). The ε_p was calculated for six clouds whose vertical velocity data at the cloud-base level were deduced by dual-Doppler analysis throughout their lifetime. The ε_p ranged from 0.03% to 9.31% and exhibited a strong positive correlation with the EA_{max}. This indicates that more than 90% of the water vapor that enters the clouds through the cloud base is consumed to moisten the atmosphere and less than 10% is converted to precipitation and returned to the ground. The cumulonimbus clouds in the region far south from the mei-yu front over the eastern Asian continent efficiently transport water vertically and humidify the upper troposphere.

1. Introduction

A cumulonimbus cloud converges water vapor from its surroundings in the lower troposphere and transports it to the upper atmosphere. Some parts of the water vapor return to the ground as rain, and others humidify the atmosphere. This water division by the cumulonimbus clouds is a fundamental element in atmospheric water circulation. Rainfall amount of cumulonimbus clouds is an essential product in this water circulation.

Several factors that have a close relationship with the convective rainfall amount have been reported in various regions, such as South Dakota (Dennis et al. 1975), North Dakota (Doneaud et al. 1981, 1984), Florida (Gagin et al. 1985), Thailand (Rosenfeld and Woodley 2003), and Israel and South Africa (Rosenfeld and Gagin 1989). For example, the horizontal and vertical dimensions have been shown as a dominant factor in the determination of the rainfall amount of cumulonimbus clouds (e.g., Dennis et al. 1975). Lopez (1978) suggested that the average size and duration of the cumu-

* Current affiliation: Okinawa Subtropical Environment Remote-Sensing Center, National Institute of Information and Communications Technology, Okinawa, Japan.

Corresponding author address: Yukari Shusse, Okinawa Subtropical Environment Remote-Sensing Center, National Institute of Information and Communications Technology, 4484 Aza-Onna, Onna, Kunigami, Okinawa 904-0411, Japan.
E-mail: shusse@nict.go.jp

© 2006 American Meteorological Society

lonimbus clouds depend on the instantaneous number of convective cells in the cloud and the total number of cells during the lifetime of the cumulonimbus cloud. Gagin et al. (1985) showed that rainfall intensity, maximum precipitation area, duration, and total rainfall amount of convective cells strongly depend on the depth of convective cells. It has also been reported that the convective cells composing multicellular cumulonimbus clouds produce a larger amount of rainfall than those of single-cell clouds (Lopez 1978; Rosenfeld and Gagin 1989). These studies suggest that the dimension of the cumulonimbus clouds, which is good indicator of rainfall of the cumulonimbus clouds, have a close relationship with the number and precipitation properties of convective cells constituting the cumulonimbus clouds. In this study, precipitation properties of cumulonimbus clouds and those of convective cells included in the clouds are investigated and summarized as dimension characteristics of cumulonimbus clouds.

Precipitation efficiency (ε_p) is one of the important parameters to evaluate the characteristics of cumulonimbus clouds. Several definitions of ε_p have been used in previous studies. Many observational studies of an isolated cumulonimbus cloud defined ε_p as the ratio of surface rainfall to the water vapor amount ingested into the cloud through the cloud base (e.g., Braham 1952; Auer and Marwitz 1968; Fankhauser 1988). In numerical studies such as Weisman and Klemp (1982) and Ferrier et al. (1996), the ε_p is calculated as the ratio of total rainfall to total condensation. In the present study, the former definition of ε_p will be used because it gives the partition ratio of the water vapor taken into cumulonimbus clouds as rainfall at the ground and the humidification of the atmosphere.

Foote and Fankhauser (1973) found that the ε_p depends on the stage of development of cumulonimbus clouds. Theoretically, the rainfall and water vapor amount in the calculation of the ε_p should be integrated over the lifetime of cumulonimbus clouds. However, it is difficult to measure them with acceptable accuracy because their time and space variations are very large. For example, most previous studies calculating the ε_p of isolated cumulonimbus clouds (e.g., Braham 1952; Auer and Marwitz 1968; Fankhauser 1971, 1988; Foote and Fankhauser 1973) used data obtained from research aircrafts in the evaluation of the water vapor flux. Using this method, it takes from ~30 min to 1 h to observe the three-dimensional moisture and wind fields of the clouds. These studies have determined the ε_p using instantaneous or partial measurements of water vapor flux with the assumption that the clouds are steady during the observation and in their mature stage.

Although there are restrictions in the observation and assumptions in the analysis described above, the dependence of the ε_p on the environmental factors, the cloud dimensions, and the internal structure of the cloud has been proposed. Marwitz (1972) showed that the ε_p of cumulonimbus clouds on the High Plains is in inverse proportion to the environmental vertical shear. Fankhauser (1988) pointed out that the ε_p is not simply in inverse proportion to the vertical shear. In his study, the mixing ratio in the subcloud layer, the shear kinetic energy in the lower troposphere, and the cloud-base area all exhibit weak positive correlations with the ε_p, while clouds with high cloud bases have a tendency to show a slight inverse correlation. Using a two-dimensional cloud model, Ferrier et al. (1996) suggested that the vertical orientation of the updrafts within clouds is an important factor to determine the ε_p. These studies have shown many important properties of the ε_p of cumulonimbus clouds under various ambient atmospheric conditions. However, the ε_p of cumulonimbus clouds with various dimensions in the same synoptic situation has not been sufficiently investigated. We still do not fully understand the relation of the ε_p to the dimension characteristics of cumulonimbus clouds.

Over continental China, cumulonimbus clouds often occur in the region far south from the mei-yu front, which is a significant subtropical frontal zone in East Asia, and under the influence of the subtropical high (Kato et al. 1995; Nakai and Kawamura 1998; Shinoda and Uyeda 2002). The dimension characteristics and ε_p of cumulonimbus clouds are basic parameters in understanding the vertical water transportation in the region where the northward horizontal transportation of water vapor to the mei-yu front is significant. In addition, the atmospheric condition in this region is relatively simple, that is, weak large-scale convergence, weak baroclinicity, and weak vertical wind shear with abundant water vapor, especially in the low levels. The clouds in this region are suitable for investigating the general properties of ordinary cumulonimbus clouds.

In July 1998, during the Global Energy and Water Cycle Experiment (GEWEX) Asian Monsoon Experiment/Huaihe River Basin Experiment (GAME/HUBEX) Intensive Field Observation (IFO), 23 isolated cumulonimbus clouds were observed by three X-band Doppler radars of Nagoya University and Hokkaido University installed in Anhui province, China. The observation area was located in the region far south from the mei-yu front during the study period. The purpose of the present study is to evaluate the dimension characteristics and ε_p of cumulonimbus clouds in the humid subtropical air mass over the eastern Asian continent.

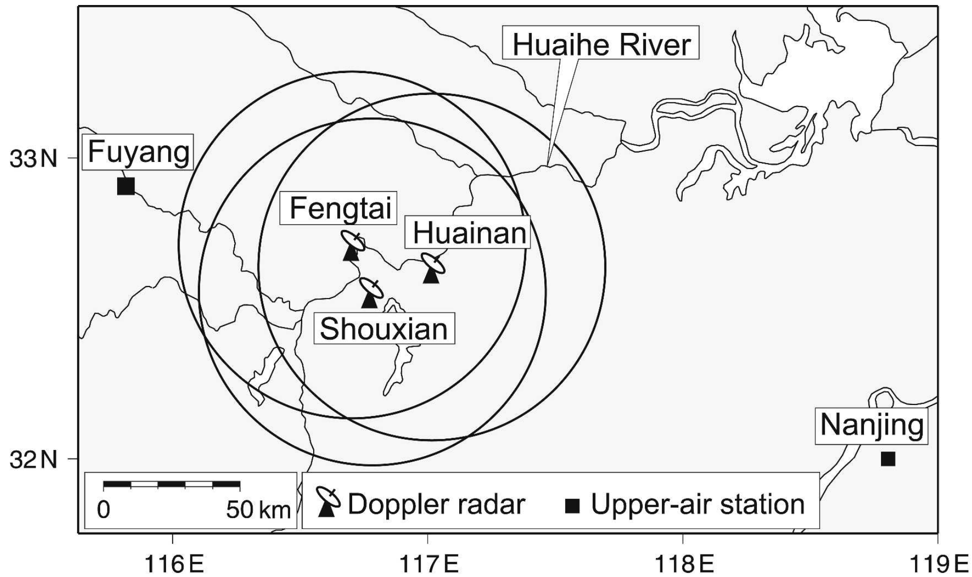

FIG. 1. Doppler radar observation sites and upper-air sounding stations. The circles show the observation ranges of Doppler radars. The location of the map region is shown in Fig. 2.

2. Observation and data

a. Radar observations and data

The GAME/HUBEX IFO was carried out in June and July 1998 in the Huaihe River basin and its surrounding area in China. Three X-band Doppler radars were operated during the GAME/HUBEX IFO. Two Doppler radars from Nagoya University were installed at Shouxian and Fengtai, China, and the Doppler radar from Hokkaido University was installed at Huainan, China (Fig. 1). The maximum quantitative observation range of each Doppler radar was 64 km. The sampling resolution of the radar data was 250 m in the radial direction and 1° in the azimuthal direction. Doppler radars were operated in plan position indicator (PPI) scanning mode at the following elevation angles in less than 7 min: 0.5°, 1.1°, 1.8°, 2.6°, 3.7°, 4.8°, 6.6°, 8.8°, 11.6°, 15.4°, 20.2°, 26.3°, 33.7°, and 40.9°. Radar reflectivity data from the Shouxian radar provide the distributions of precipitation in this paper. Three-dimensional wind fields were derived from the Shouxian, Fengtai, and Huainan radars.

The reflectivity values for the Shouxian radar were corrected for the attenuation due to precipitation using the following *K–R* relationship (Doviak and Zrnić 1984):

$$K = 0.01R^{1.21}, \tag{1}$$

where K is the attenuation rate (dB km^{-1}) and R is the rainfall intensity (mm h^{-1}). The R values were evaluated using the *Z–R* relationships

$$Z = BR^{\beta}, \tag{2}$$

where Z is the radar reflectivity factor (mm^6 m^{-3}). The adequate values of B and β in this study will be discussed later.

Doppler velocities and corrected radar reflectivity factors were interpolated to grid points with vertical and horizontal intervals of 500 m in Cartesian coordinates using the Cressman weighting function (Cressman 1959). A correction related to the movement of radar echoes was made using Gal-Chen's method (Gal-Chen 1982). The vertical velocity was determined by the upward integration of the anelastic continuity equation using the boundary condition of 0 m s^{-1} at the ground. The vertical velocity w used in the present analysis was only at the cloud-base level (1.5 km AGL as defined later). The error of w is not serious at this level when using this evaluation method.

Upper-air sounding data at the Fuyang Meteorological Observatory, which is located 100 km northwestward from the Shouxian Doppler radar site, was used to describe the general environmental characteristics.

b. Radar rainfall estimates

For the rainfall estimation, the radar reflectivity factor Z (mm^6 m^{-3}) was converted into rainfall intensity R (mm h^{-1}) using (2). In this study, the Jones (1956) relation $Z = 486\,R^{1.37}$ for cumulonimbus clouds in Illinois was used in the rainfall estimation. This *Z–R* relation was chosen because the geography (over the continent) and type of rain (convective) are similar to those of the present cases.

3. The atmospheric conditions

Figure 2 shows the surface weather map at 1400 LST (LST = UTC + 8 h) on 10, 11, and 13 July 1998. On 10 July, the mei-yu front was located about 500 km north of the observation site and extended zonally (Fig. 2a). The mei-yu front shifted eastward on 11 July (Fig. 2b). A low appeared near 40°N, 105°E on 12 July (not shown). The center of the low was located near 44°N, 113°E on 13 July (Fig. 2c). Its trailing cold and warm fronts extended southwestward and southeastward, respectively. Doppler radar observation sites were located about 1000 km away southward from the low center. Geostationary Meteorolgical Satellite (GMS) infrared imagery shows that the observation area of the Doppler radars was not covered with a synoptic-scale cloud system around 1400 LST on 10, 11, and 13 July (not shown).

Figure 3 shows the vertical profiles of temperature and dewpoint temperature observed at 1400 LST on 10, 11, and 13 July at Fuyang, China. During the 3 days, the air temperature reached 35°C, and the water vapor mixing ratio was about 20 g kg^{-1} (not shown) at the surface. The relative humidity was less than 30% at 6 km on 10 July, less than 50% at 5 km on 11 July, and less than 40% at 3 km on 13 July. Some parameters of the profiles in Fig. 3 are summarized in Table 1. The lifting condensation level (LCL), the level of free convection (LFC), and the convective available potential energy (CAPE) were determined by a parcel of the lowest 50 hPa of the soundings. The LCLs during the 3 days did not show large differences and ranged from 1350 to 1510 m. The LFC on 13 July was 2200 m, somewhat higher than those of the two other days, 1530 and 1380 m. The CAPEs were 940, 2730, and 2230 J kg^{-1} on 10, 11, and 13 July, respectively. The freezing level and precipitable water (Pwat) amount ranged from 5270 to 5880 m and from 55 to 59 mm, respectively. The low-level vertical wind shear between the surface and 5 km AGL was weak, less than 2.0×10^{-3} s^{-1} during the 3 days. The atmospheres observed at Fuyang during the 3 days were generally almost the same and were convectively unstable enough for cumulonimbus clouds to develop.

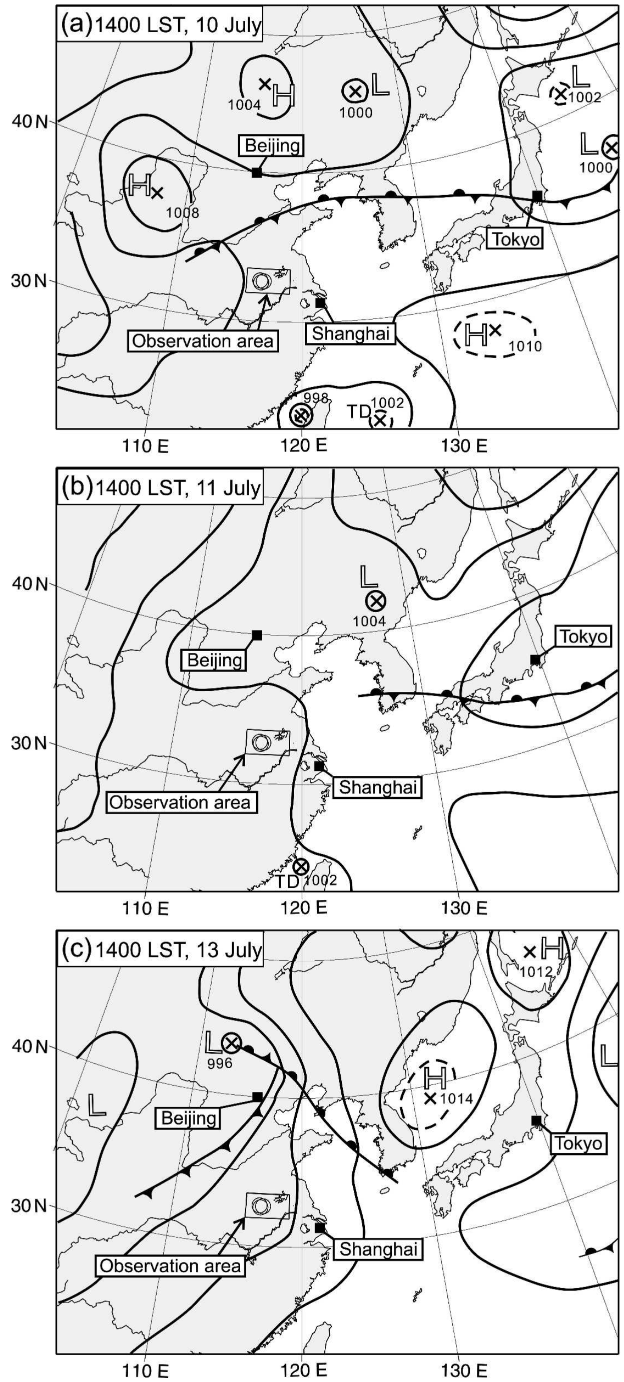

FIG. 2. Surface weather map at 1400 LST on (a) 10, (b) 11, and (c) 13 Jul 1998. The frame of Fig. 1 is shown by the rectangle in the figure.

4. Dimension characteristics of convective echoes

In this paper, convective echoes stronger than 10 dB*Z* at 0.5 km AGL were used for the analysis. During the 3 days, 23 convective echoes were observed, and they corresponded to cumulonimbus clouds. All convective echoes occurred in the afternoon. Each convective echo was tracked within the observation range. Most convective echoes were observed from their appearance to their disappearance. One exception, which

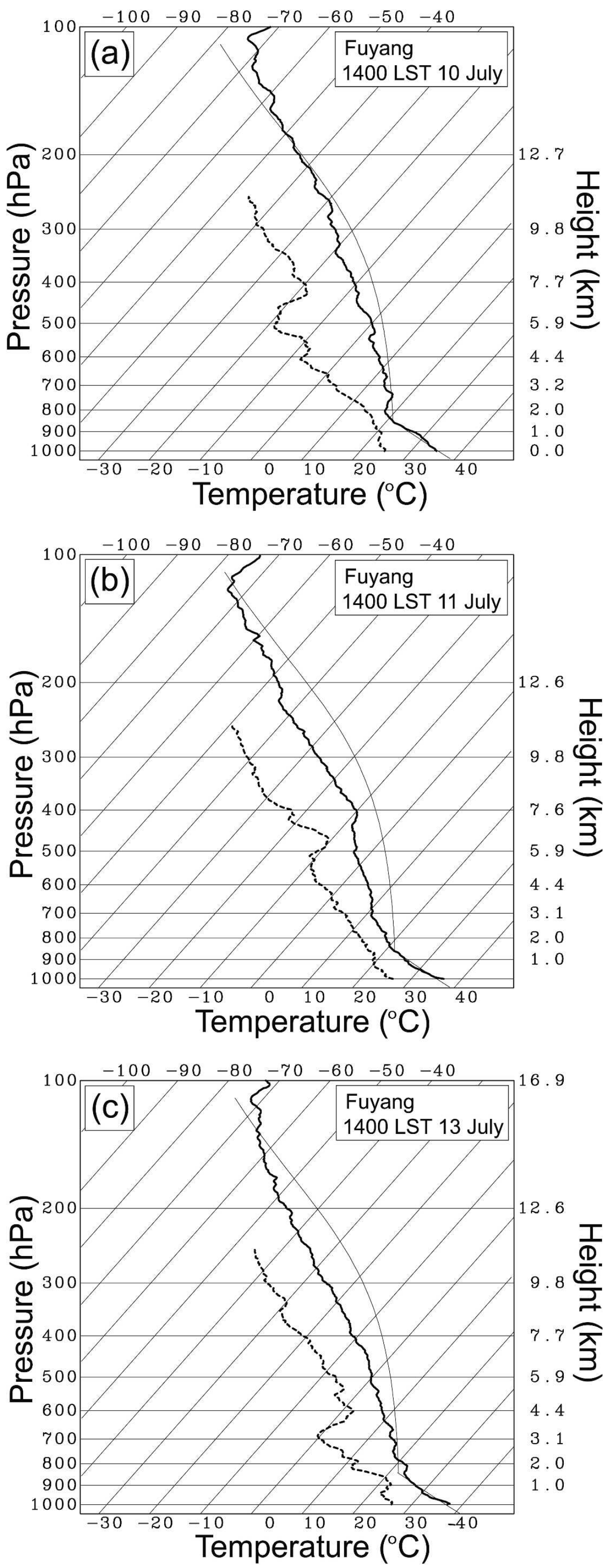

FIG. 3. Vertical profiles of temperature (thick solid line) and dewpoint temperature (dashed line) observed at Fuyang at 1400 LST on (a) 10, (b) 11, and (c) 13 Jul 1998. A thin solid line

←

indicates the path of a moist-adiabatic ascent of the air having the averaged properties of the lowest 50 hPa of the individual soundings.

TABLE 1. Characteristic parameters of the soundings shown in Fig. 3.

	LCL (m)	LFC (m)	Freezing level (m)	Pwat (mm)	CAPE (J kg^{-1})
10 Jul	1490	1530	5900	55	940
11 Jul	1350	1380	5270	56	2730
13 Jul	1510	2200	5880	59	2230

went out of the observation range before its dissipation, was the most vigorous and largest convective echo among the echoes observed during the 3 days. The detailed three-dimensional structure of this convective echo is described in Shusse et al. (2005). For this convective echo, the 1.5-h period of observation, which contains the developing and mature stages, was used in the present analysis.

A typical convective echo in the present analysis is illustrated in Fig. 4a using a sequence of horizontal echo distribution at 0.5 km AGL. The convective echo was observed first at 1245 LST on 10 July. In this study, convective cells are defined as reflectivity maxima at 0.5 km AGL. One to three convective cells were found within the convective echo at each time. The total number of cells (TNC) during the lifetime of the convective echo was five. They are labeled from 1 to 5 in the order of their formation and tracked in Fig. 4a. The convective echo did not show the regular formation of new cells. This is an ordinary evolution of cumulonimbus clouds under a weak vertical wind shear condition. The convective echo did not accompany the broad stratiform precipitation at low levels.

Figure 4b shows the time variation of the echo area at 0.5 km AGL and the echo-top height of the convective echo shown in Fig. 4a. Both the echo area and the echo-top height gradually increased and then decreased. The maximum echo area at 0.5 km AGL (EA_{max}) was 69 km^2 at 1320 LST. The maximum echo top (ET_{max}) was 10.5 km AGL at 1306 LST. The EA_{max} was observed following the ET_{max}. These features were common to almost all the analyzed convective echoes. The lifetime of the convective echo was 63 min. The lifetime was estimated by adding 3.5 min before the first observation and after the last observation of each convective echo.

Figure 5 shows the scatterplot of the EA_{max} and ET_{max} of the 23 convective echoes. The EA_{max} and

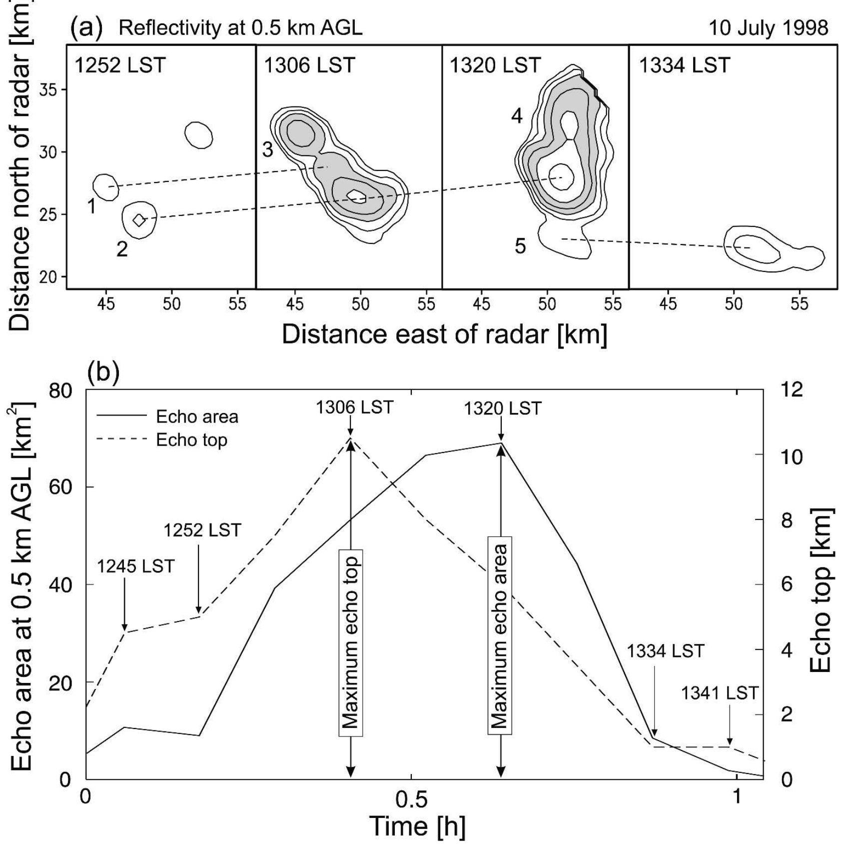

FIG. 4. (a) Time series of the constant altitude PPI (CAPPI) display of the radar echo of a convective echo at 0.5 km AGL observed on 10 Jul 1998. The contours of the radar echo intensity are drawn every 5 dBZ from 10 dBZ. Areas from 20 to 30 dBZ are shaded. Convective cells are labeled from 1 to 5 in the order of their formation and tracked in the figure. (b) Time variations of the horizontal echo area above 10 dBZ at 0.5 km AGL (solid line) and the echo-top height (dashed line) of the convective echo illustrated in (a).

ET_{max} ranged from 0.5 to 470 km^2 and from 2 to 19 km, respectively. They showed a linear relationship on the logarithmic plot. The open circles on the dots in Fig. 5 indicate convective echoes with a single cell throughout their lifetime. They are, hereafter, referred to as "single-cell echoes." Nine of the 23 convective echoes are single-cell echoes. The largest single-cell echo showed an EA_{max} of 41 km^2. The ET_{max} of the tallest single-cell echo was 8 km AGL. All of the echoes reaching 10 km AGL were multicellular echoes. In other words, deep cells reaching 10 km AGL developed only within multicellular echoes. The lifetimes of single-cell echoes were less than 40 min. The open squares in Fig. 5 indicate convective echoes that were maintained for more than 1 h. Most multicellular echoes were maintained for more than 1 h and lasted less than 2.5 h.

Figure 6 shows the TNC as a function of the EA_{max}. The TNC of individual convective echoes ranged from 1 to 25. All convective echoes smaller than 10 km^2 in EA_{max} were single-cell echoes. Roughly, the TNC increases with the EA_{max}.

The area time integral (ATI) is a measure of the rainfall area coverage and duration. This has been presented as a useful parameter for the total rainfall amount of an individual convective echo (e.g., Doneaud et al. 1981, 1984; Atlas et al. 1990; Rosenfeld et al. 1990; Johnson et al. 1994; Li and Senesi 1997). The ATI is defined as

$$\mathrm{ATI} = \int_T A(t)\,dt, \tag{3}$$

where $A(t)$ is the area of the convective echoes at 0.5 km AGL. Here, ATI is used as a parameter that shows the scale of convective echoes. To clarify the relationship between the scale of convective echoes and the averaged scale of cells within convective echoes, the

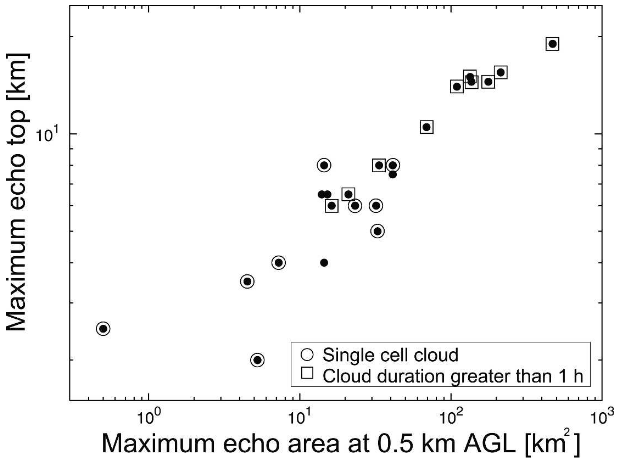

FIG. 5. Scatterplot of the maximum echo area at 0.5 km AGL (EA_{max}) and the maximum echo top (ET_{max}). Open circles upon the dots indicate a single-cell echo. Open squares mean that the lifetime of convective echoes is longer than 1 h.

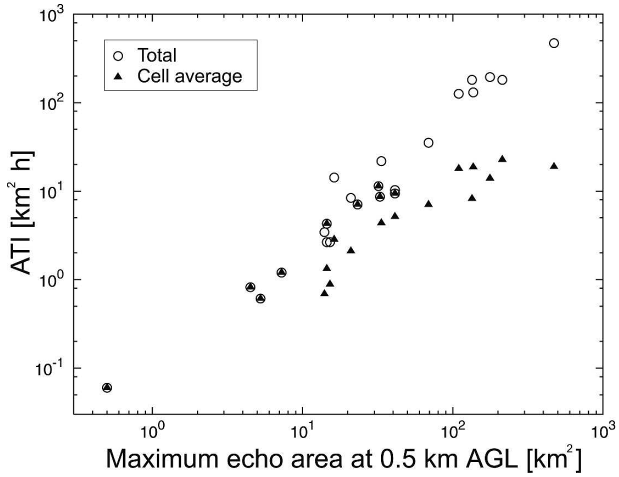

FIG. 7. The ATI (closed triangles) and cell-averaged ATI (ATI_{cell} = ATI/TNC) (open circles) as a function of the maximum echo area at 0.5 km AGL (EA_{max}).

ATI is divided by the TNC. This is referred to as a cell-averaged ATI (ATI_{cell} = ATI/TNC). Figure 7 shows the ATI and ATI_{cell} (km^2 h) as a function of the EA_{max}. The ATI has a linear dependence on the EA_{max} on the logarithmic plot. The ATI_{cell} also increases with an EA_{max} smaller than 100 km^2. On the other hand, the ATI_{cell} approaches a constant value of about 20 km^2 h with an EA_{max} larger than 100 km^2. This indicates that there is an upper bound of the ATI_{cell}, while the ATI increase with the EA_{max} throughout the range.

Figure 8 shows the scatterplot of the maximum rainfall intensity (RI_{max}) with the EA_{max}. The RI_{max} ranges from 0.06 to 35.0 mm h^{-1}. On the logarithmic plot, the RI_{max} increases with an EA_{max} smaller than 100 km^2. The RI_{max} is almost constant with an EA_{max} larger than 100 km^2.

An estimation of the total rainfall amount (R_{tot}) was made from the radar rainfall data at 0.5 km AGL according to

$$R_{tot} = \rho_w \int_T \int_A R \, dA \, dt, \tag{4}$$

where R is the rainfall intensity and ρ_w is the density of water. The integration in (4) is performed over the entire area and over the lifetime of each convective echo. The R_{tot} of the convective echoes ranged from 3.5×10^3 to 9.0×10^8 kg. Figure 9 shows the relationships of the R_{tot} to the EA_{max} (Fig. 9a), ET_{max} (Fig. 9b), and ATI

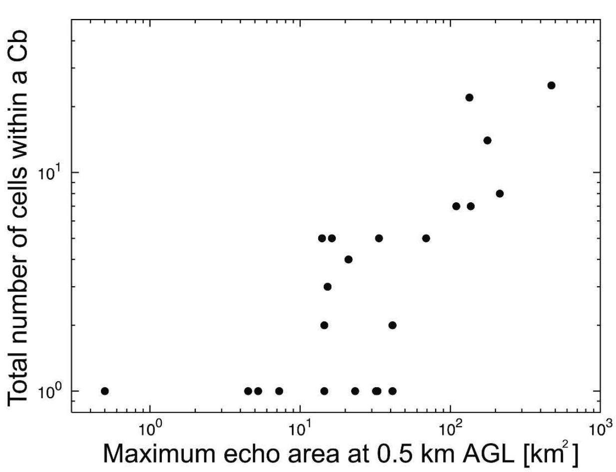

FIG. 6. The TNC within convective echoes over their lifetime as a function of the maximum echo area at 0.5 km AGL (EA_{max}).

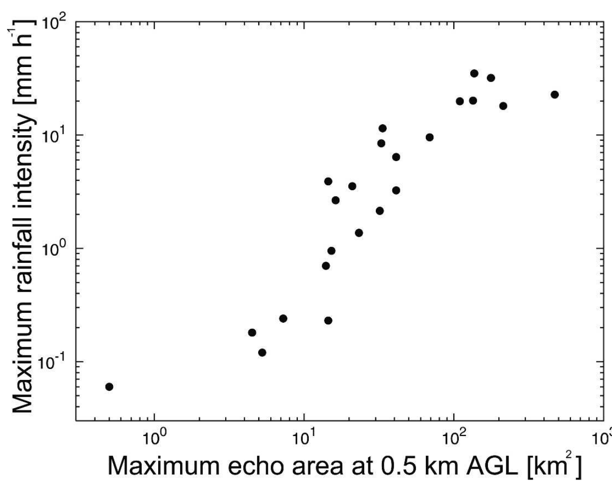

FIG. 8. Scatterplot of the maximum rainfall intensity (RI_{max}) and the maximum echo area at 0.5 km AGL (EA_{max}).

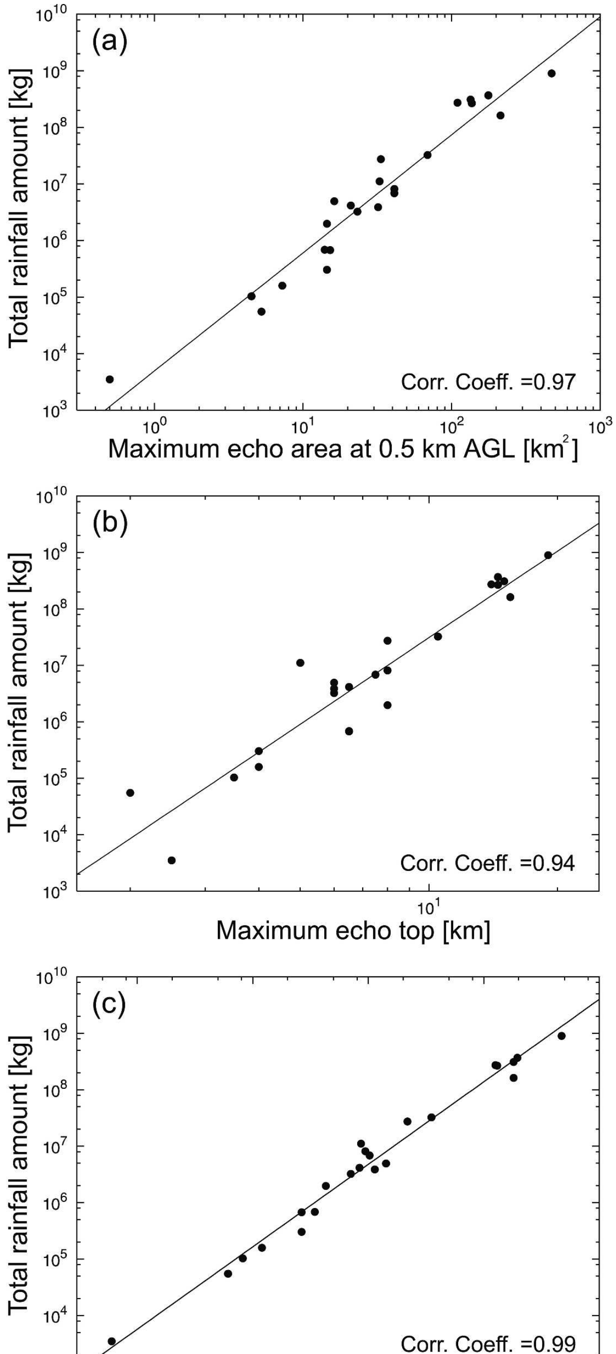

FIG. 9. Relationship of the total rainfall amount (R_{tot}) to (a) the maximum echo area at 0.5 km AGL (EA_{max}), (b) the maximum echo top (ET_{max}), and (c) the maximum rainfall intensity (RI_{max}).

(Fig. 9c). The R_{tot} is well correlated with these three parameters. The correlation coefficients between the R_{tot} and EA_{max}, ET_{max}, and ATI are 0.97, 0.94, and 0.99, respectively. These high correlation coefficients

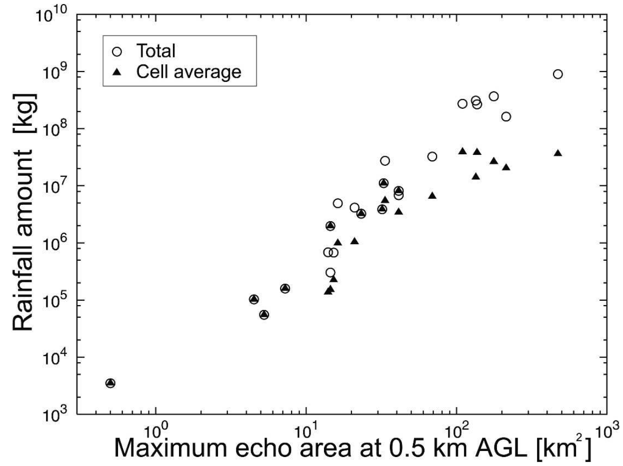

FIG. 10. Relationship of the cell-averaged rainfall amount (R_{cell} = R_{tot}/TNC) to the maximum echo area at 0.5 km AGL (EA_{max}). The total rainfall amount (R_{tot}) is also plotted.

indicate that the R_{tot} strongly depends on the dimensions of the convective echoes.

The R_{tot} is divided by the TNC in order to investigate the averaged rain productivity of cells within each convective echo. This is referred to as the cell-averaged rainfall amount (R_{cell}). Figure 10 shows the relationship between the R_{cell} and the EA_{max}. The R_{cell} increases with an EA_{max} smaller than 100 km^2. On the other hand, the R_{cell} approaches a constant value of about 4.0×10^7 kg for an EA_{max} larger than 100 km^2. There is an upper bound of the R_{cell} of the convective echoes.

In summary, the maximum echo height (ET_{max}), TNC, ATI, and total rainfall amount (R_{tot}) are strongly dependent on the maximum echo area (EA_{max}) of convective echoes. On the other hand, the cell-averaged ATI (ATI_{cell}), maximum rainfall intensity (RI_{max}), and cell-averaged rainfall amount (R_{cell}) increase with an EA_{max} smaller than 100 km^2, while they show almost constant values with an EA_{max} larger than 100 km^2.

5. Precipitation efficiency

In the present study, precipitation efficiency (ε_p) is defined as

$$\varepsilon_p = \frac{R_{tot}}{V_{tot}}, \tag{5}$$

where V_{tot} is the total water vapor amount ingested into the cloud through the cloud base over its lifetime, which is the main water source for cumulonimbus clouds. The V_{tot} is given by

$$V_{tot} = \rho_a q_v \int_T \int_A w \, dA \, dt, (w > 0), \tag{6}$$

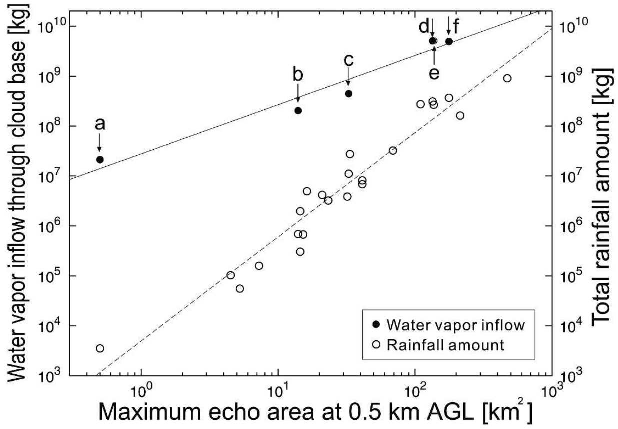

FIG. 11. Relationship of the total water vapor inflow at the cloud base (V_{tot}) to the maximum echo area at 0.5 km AGL (EA_{max}). The total rainfall amount (R_{tot}) is also plotted. Solid and dashed lines indicate the regression lines for V_{tot} and R_{tot}, respectively.

where ρ_a is the atmospheric density, q_v is the water vapor mixing ratio, and w is the vertical velocity derived from dual-Doppler analysis. The integration in (6) is performed over the area of $w > 0$ within the convective echoes and over the lifetime of each convective echo. The ρ_a and q_v in (6) were derived from the upper-air sounding data at Fuyang, and it is assumed that they were horizontally uniform around the observation area. This assumption is considered to be reasonable because the surface weather maps at 1400 LST on 11 and 13 July 1998 in Fig. 2 show that no significant synoptic-scale disturbance was present within the observation area of the Doppler radars. The vertical velocity data at cloud-base level were obtained for six convective echoes on 11 and 13 July almost over their lifetime, and their V_{tot} was calculated. Since the LCLs were 1350 and 1510 m AGL at 1400 LST on 11 and 13 July at Fuyang, respectively, the w, ρ_a, and q_v at 1.5 km AGL were used in the calculation of the V_{tot} under the assumption that the cloud-base levels were comparable with LCLs.

Figure 11 shows the relationship between V_{tot} and the EA_{max}. The R_{tot} and its regression line are also shown in the figure for reference. It is found that the V_{tot} has a linear relation with the EA_{max}. The regression line of the V_{tot} and that of the R_{tot} approach each other as the EA_{max} increases. This indicates that the ratio of the R_{tot} to the V_{tot} increases with an EA_{max} in the range of the convective echoes presented here. From this relationship between V_{tot} and R_{tot}, ε_p is expected to increase with the EA_{max}.

The ε_p is calculated for the six convective echoes whose V_{tot} is presented in Fig. 11. They were labeled from "a" to "f" in the order of their EA_{max}. In the estimation of the ε_p for each convective echo, various Z–R relationships were used to examine the variations of ε_p due to the Z–R relationships. Table 2 summarizes the ε_p of the six convective echoes by each Z–R relationship and their averages. The variations associated with the Z–R relationships tend to increase with the EA_{max}, and they are 0.02% and 5.3% in the smallest and largest convective echoes (a and f) among the six convective echoes, respectively.

The ε_p is plotted in Fig. 12 as a function of the EA_{max}. The error bars in the figure indicate the range associated with the choice of Z–R relationships listed in Table 2. Solid circles indicate their averages. The ε_p generally becomes large with the EA_{max}. The averaged ε_p ranges from 0.03% to 9.31%. These precipitation efficiencies in the present study indicate that more than 90% of the water vapor that entered the clouds through the cloud base is consumed to moisten the atmosphere and less than 10% is converted to precipitation and returned to the ground.

6. Discussion

a. Dimension characteristics of cumulonimbus clouds

As summarized in section 4, the maximum echo height (ET_{max}), *TNC*, ATI, and total rainfall amount (R_{tot}) are strongly dependent on the maximum echo area (EA_{max}) of cumulonimbus clouds. On the other hand, the cell-averaged ATI (ATI_{cell}), maximum rainfall intensity (RI_{max}), and cell-averaged rainfall amount (R_{cell}) increase when the EA_{max} is smaller than 100 km^2 and are almost constant when the EA_{max} is larger than 100 km^2. On the basis of these relationships, the cumulonimbus clouds studied in the present paper are clas-

TABLE 2. Precipitation efficiencies (%) of convective echoes a, b, c, d, e, and f derived from each Z–R relationship.

		a	b	c	d	e	f
Jones (1956)	$Z = 486R^{1.37}$	0.02	0.34	2.49	6.08	5.24	7.47
Fujiwara (1965)	$Z = 450R^{1.46}$	0.02	0.39	2.49	5.92	5.01	7.18
Doviak and Zrnić (1984)	$Z = 400R^{1.4}$	0.02	0.40	2.82	6.85	5.89	8.40
Imai (1960)	$Z = 200R^{1.5}$	0.04	0.71	4.22	10.26	8.75	12.52
Marshall and Palmer (1948)	$Z = 200R^{1.6}$	0.04	0.73	3.87	9.12	7.60	10.97
Avg		0.03	0.51	3.18	7.65	6.49	9.31

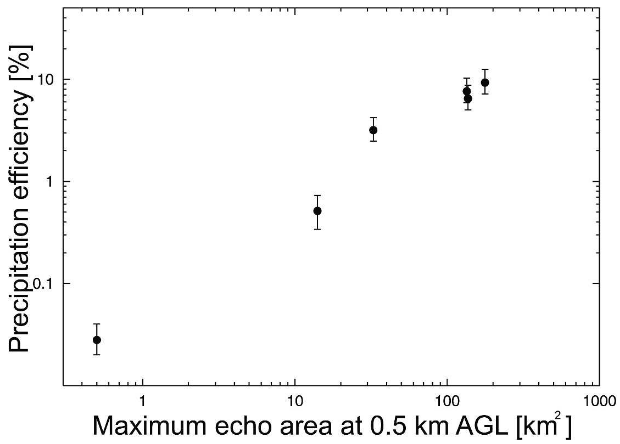

FIG. 12. Scatterplot of the precipitation efficiency (ε_p) and the maximum echo area at 0.5 km AGL (EA_{max}). Error bars indicate the range associated with the choice of *Z–R* relationships listed in Table 2. Solid circles indicate their average.

sified into two scales according to the EA_{max}: small cumulonimbus clouds (<100 km^2 in EA_{max}) and large cumulonimbus clouds (>100 km^2 in EA_{max}).

The small cumulonimbus clouds are single-cell clouds or small multicellular clouds whose TNC are no more than 5. In the small cumulonimbus clouds, both the ATI and ATI_{cell} increase with the EA_{max}. This indicates that the area and lifetime of small cumulonimbus clouds have a close relationship with those of cells within small cumulonimbus clouds. The R_{cell} also increases with the EA_{max}. The rain productivity of small cumulonimbus clouds increases not only by the increase of the TNC but also by the intensification of cells.

The large cumulonimbus clouds are large multicellular clouds whose TNC are more than 5. In the large cumulonimbus clouds, there is an upper bound of the ATI_{cell}. This indicates that the area and lifetime of large cumulonimbus clouds depend on the TNC rather than on the average scale of cells within the clouds. The R_{cell} also show almost constant values in large cumulonimbus clouds. These facts indicate that large cumulonimbus clouds increase their rain productivity by the increase of the TNC rather than by the intensification of cells.

Rosenfeld and Gagin (1989) showed similar results that a significant change in cell area-time integrated rain volume was not found in cell cluster with much number of cells, while cell area-time integrated rain volume tends to depend generally on the number of cells in the cluster in which the subject cell resides. It seems to be the common property that there is an upper bound for an increase in rainfall amount from cells with the expansion of an area of cell-clustered clouds. The significance in the present study is that these precipitation properties of convective cells are summarized as dimension characteristics of cumulonimbus clouds.

b. *Relationship between the precipitation efficiency and dimension characteristics*

There have been few studies examining the relationship between the precipitation efficiency (ε_p) and dimension characteristics of cumulonimbus clouds based on the observation results. Fankhauser (1988) showed a weak positive correlation of the ε_p and cloud-base area of cumulonimbus clouds observed in various atmospheric situations. In the present study, the clouds developed under almost the same synoptic condition. The difference in the ε_p among the cumulonimbus clouds shown in Fig. 12 is considered to be mainly due to the dimension characteristics of the clouds.

The ε_p exhibits a strong positive correlation with the EA_{max}, as shown in Fig. 12, and ranges from 0.03% to 9.31%. This positive correlation is attributed to the fact that the dilution rate of the air within the clouds by entrainment is generally inversely proportional to the radius of clouds, as stated in Braham (1952) and Fankhauser (1988). From another viewpoint, it can be said that the ε_p increases with the TNC because the TNC increases with the EA_{max}. A cell that preexisted in a multicellular cloud locally humidifies its surrounding. This humidification would reduce the effect of the entrainment of dry air for subsequent cells in the cloud. In addition, when several cells exist simultaneously in a multicellular cloud, a cell located in the central part of the cloud is defended from the entrainment of dry air by the surrounding cells. These local modifications within and around the multicellular clouds seem to be important for the increase of the ε_p. This local humidification could be one of the reasons that cells reach 10 km AGL only within multicellular clouds.

The cumulonimbus clouds in the present study become large with the TNC, and the EA_{max} of the largest cumulonimbus cloud was 470 km^2. This is likely to be the maximum extent for isolated cumulonimbus clouds under the present atmospheric condition. It is inferred from the relationship between the regression lines for the V_{tot} and R_{tot} in Fig. 11 that the ε_p (the ratio of the R_{tot} to the V_{tot}) is about 15% for a cumulonimbus cloud with an EA_{max} of about 470 km^2. It is reasonable to suppose that the ε_p of isolated cumulonimbus clouds in the region far south from the mei-yu front over the eastern Asian continent is at most 15%.

c. *Comparison with previous studies of precipitation efficiency*

The precipitation efficiency (ε_p) of cumulonimbus clouds has been investigated in various areas. Braham

(1952) calculated an ε_p of approximately 10% for small airmass cumulonimbus clouds with a typical lifetime of 25 min in Florida and Ohio. Marwitz (1972) summarized the ε_p of cumulonimbus clouds over the Great Plains, which was 5%–120%. The ε_p higher than 100% in his study is probably caused by using instantaneous or partial measurements and owing to insufficient time to integrate observation data. Fankhauser (1988) estimated an ε_p of about 20%–50% for cumulonimbus clouds with a cloud-base area ranging from 100 to 1000 km^2 observed in Montana. Ferrier et al. (1996) showed the ε_p in simulated midlatitude and tropical squall lines, which ranged from 20% to 50% in terms of rainfall divided by condensation.

In the present analysis, the ε_p was integrated over the lifetime of the cumulonimbus clouds using the Doppler radar data resolved at interval of 7 min. The ε_p ranged from 0.03% to 9.31%. This indicates that more than 90% of the water vapor that entered the clouds through the cloud base is consumed to moisten the surrounding atmosphere. It seems that the entrainment process is dominant in these clouds because the dry air was present above LCL in the environment during the period as shown in Fig. 3. The large mixing ratio at the lower levels was also important for the supply of water to the upper levels. Abundant water vapor at the low levels and relatively dry air at the upper levels results in the low precipitation efficiency of clouds in this region. It can be said that cumulonimbus clouds in the region far south from the mei-yu front over the eastern Asian continent work very efficiently to transport water vertically and humidify the upper atmosphere.

7. Summary

The dimension characteristics and precipitation efficiency of cumulonimbus clouds observed during 3 days in July 1998 in Anhui province, China, were studied mainly using reflectivity and wind data of X-band Doppler radars and upper-air sounding data during the GAME/HUBEX IFO. During the 3 days, the observation area was situated in the region far south from the mei-yu front and to the west of the subtropical high. The air temperature reached 35°C in the daytime and the water vapor mixing ratio was about 20 g kg^{-1} at the surface. The lifting condensation levels were 1.3–1.5 km. The vertical wind shear in the lower level was weak, less than 2.0×10^{-3} s^{-1}. The atmospheric condition was convectively unstable enough for cumulonimbus clouds to develop.

Twenty-three cumulonimbus clouds were identified and tracked over their lifetime. The characteristics of the cumulonimbus clouds are summarized as follows. The maximum echo area (EA_{max}) ranged from 0.5 to 470 km^2. The maximum echo top (ET_{max}) ranged from 2 to 19 km. The cumulonimbus clouds comprised one to several convective cells at the same time. The total number of cells (TNC) within the cumulonimbus clouds over their lifetime was from 1 to 25. Cells reaching 10 km AGL developed only within multicellular cumulonimbus clouds. The durations of single-cell clouds were less than 40 min. Many of the multicellular clouds were maintained for more than 1 h and lasted less than 2.5 h. The maximum rainfall intensity (RI_{max}) ranged from 0.06 to 35.0 mm h^{-1}, and the total rainfall amount (R_{tot}) ranged from 3.5×10^3 to 9.0×10^8 kg.

The ET_{max}, TNC, area time integral (ATI), and R_{tot} were strongly dependent on the EA_{max}. In contrast, the cell-averaged ATI (ATI_{cell} = ATI/TNC), RI_{max}, and cell-averaged rainfall amount ($R_{cell} = R_{tot}$/TNC) increased with an EA_{max} smaller than 100 km^2 and were almost constant with an EA_{max} larger than 100 km^2. On the basis of these relationships, the cumulonimbus clouds studied in the present paper were classified into two scales according to the EA_{max}: small cumulonimbus clouds (<100 km^2 in EA_{max}) and large cumulonimbus clouds (>100 km^2 in EA_{max}).

In small cumulonimbus clouds, the area and lifetime of the clouds have a close relationship with those of cells within the clouds. The rain productivity of small cumulonimbus clouds increases not only by the increase of the TNC but also by the intensification of cells. On the other hand, in large cumulonimbus clouds, the area and lifetime of the clouds depend on the TNC rather than the scale of cells within the clouds. The large cumulonimbus clouds increase the rain productivity by the increase of the TNC rather than by the intensification of cells.

The precipitation efficiency (ε_p) is defined as the ratio of surface rainfall to water vapor inflow in this paper. The ε_p was calculated for six clouds whose the vertical velocity data at the cloud-base level were deduced throughout their lifetime. The ε_p of the clouds ranged from 0.03% to 9.31% and exhibited a strong positive correlation with the EA_{max} of cumulonimbus clouds. This indicates that more than 90% of the water vapor that entered the clouds through the cloud base is consumed to moisten the surrounding atmosphere and less than 10% is converted to precipitation and returned to the ground. The cumulonimbus clouds in the region far south from the mei-yu front over the eastern Asian continent efficiently transport water vertically and humidify the upper troposphere.

Acknowledgments. The authors thank Prof. Hiroshi Uyeda, Nagoya University, for his useful suggestions and continuous encouragement throughout this study. Thanks are also due to Dr. Taro Shinoda, Nagoya University, for his fruitful discussions. The authors would also like to thank Dr. Daniel Rosenfeld and the anonymous reviewers for their useful comments. The authors are grateful to the Chinese GAME/HUBEX Project Office for providing the data of upper-air sounding. Thanks are extended to all members of the GAME/HUBEX project for their help and cooperation in the observations. We are also grateful to staff members of the Shouxian and Fengtai Meteorological Observatories and the Huainan Chaoyang Hospital for their cooperation and kind support during the field observation. This work was supported by a Grant-in-Aid for Scientific Research from the Ministry of Education, Science, Culture, and Sports of Japan. This work is dedicated to the late Prof. Takao Takeda, who was the leader of the GAME/HUBEX project.

REFERENCES

Atlas, D., D. Rosenfeld, and D. A. Short, 1990: The estimation of convective rainfall by area integrals. Part I: The theoretical and empirical basis. *J. Geophys. Res.,* **95** (D3), 2153–2160.

Auer, A. H., and J. D. Marwitz, 1968: Estimates of air and moisture flux into hailstorms on the High Plains. *J. Appl. Meteor.,* **7,** 196–198.

Braham, R. R., Jr., 1952: The water and energy budgets of the thunderstorm and their relation to thunderstorm development. *J. Meteor.,* **9,** 227–242.

Cressman, G. P., 1959: An operational objective analysis system. *Mon. Wea. Rev.,* **87,** 367–374.

Dennis, A. S., A. Koscielaki, D. E. Cain, J. H. Hirsch, and P. L. Smith Jr., 1975: Analysis of radar observations of a randomized cloud seeding experiment. *J. Appl. Meteor.,* **14,** 897–908.

Doneaud, A. A., P. L. Smith, A. S. Dennis, and S. Sengupta, 1981: A simple method for estimating convective rain volume over an area. *Water Resour. Res.,* **17,** 1676–1682.

——, S. I. Niscov, D. L. Priegnitz, and P. L. Smith, 1984: The area-time integral as an indicator for convective rain volumes. *J. Climate Appl. Meteor.,* **23,** 555–561.

Doviak, R. J., and D. S. Zrnić, 1984: *Doppler Radar and Weather Observations.* Academic Press, 458 pp.

Fankhauser, J. C., 1971: Thunderstorm–enviroment interactions determined from aircraft and radar observations. *Mon. Wea. Rev.,* **99,** 171–191.

——, 1988: Estimates of thunderstorm precipitation efficiency from field measurements in CCOPE. *Mon. Wea. Rev.,* **116,** 663–684.

Ferrier, B. S., J. Simpson, and W.-K. Tao, 1996: Factors responsible for precipitation efficiencies in midlatitude and tropical squall simulations. *Mon. Wea. Rev.,* **124,** 2100–2125.

Foote, G. B., and J. C. Fankhauser, 1973: Airflow and moisture budget beneath a north–east Colorado hailstorm. *J. Appl. Meteor.,* **12,** 1330–1353.

Fujiware, M., 1965: Raindrop-size distribution from individual storms. *J. Atmos. Sci.,* **22,** 585–591.

Gagin, A., D. Rosenfeld, and R. E. Lopez, 1985: The relationship between height and precipitation characteristics of summertime convective cells in south Florida. *J. Atmos. Sci.,* **42,** 84–94.

Gal-Chen, T., 1982: Errors in fixed and moving frame of references: Applications for conventional and Doppler radar analysis. *J. Atmos. Sci.,* **39,** 2279–2300.

Imai, I., 1960: Raindrop-size distributions and Z–R relationships. *Proc. Eighth Weather Radar Conf.,* San Francisco, CA, Amer. Meteor. Soc., 211–218.

Johnson, L. R., P. L. Smith, T. H. V. Haar, and D. Reinke, 1994: The relationship between area–time integrals determined from satellite infrared data by means of a fixed-threshold approach and convective rainfall volumes. *Mon. Wea. Rev.,* **122,** 440–448.

Jones, D. M. A., 1956: Rainfall drop-size distribution and radar reflectivity. Research Rep. 6, Meteorology Laboratory, Illinois State Water Survey, 20 pp.

Kato, K., J. Matsumoto, and H. Iwasaki, 1995: Diurnal variation of Cb-clusters over China and its relation to large-scale conditions in the summer of 1979. *J. Meteor. Soc. Japan,* **73,** 1219–1234.

Li, L., and S. Senesi, 1997: Properties of the threshold method on a radar rain cluster basis. *J. Appl. Meteor.,* **36,** 1493–1506.

Lopez, R. E., 1978: Internal structure and development processes of C-scale aggregates of cumulus clouds. *Mon. Wea. Rev.,* **106,** 1488–1494.

Marshall, J. S., and W. M. Palmer, 1948: The distribution of raindrops with size. *J. Meteor.,* **5,** 165–166.

Marwitz, J. D., 1972: Precipitation efficiency of thunderstorms on the high plains. *J. Res. Atmos.,* **6,** 367–370.

Nakai, S., and R. Kawamura, 1998: Characteristics of cloud clusters appeared around the Baiu Front: Prevailing scale of organized convection and environmental condition (in Japanese). *Tenki,* **45,** 895–905.

Rosenfeld, D., and A. Gagin, 1989: Factors governing the total rainfall yield from continental convective clouds. *J. Appl. Meteor.,* **28,** 1015–1030.

——, and W. L. Woodley, 2003: Spaceborne inferences of cloud microstructure and precipitation processes: Synthesis, insights, and implications. *Cloud Systems, Hurricanes, and the Tropical Rainfall Measuring Mission (TRMM): A Tribute to Dr. Joanne Simpson, Meteor. Monogr.,* No. 51, Amer. Meteor. Soc., 59–80.

——, D. Atlas, and D. A. Short, 1990: The estimation of convective rainfall by area integrals. Part II: The height–area rainfall threshold (HART) method. *J. Geophys. Res.,* **95** (D3), 2161–2176.

Shinoda, T., and H. Uyeda, 2002: Effective factors in the development of deep convective clouds over the wet region of eastern China during the summer monsoon season. *J. Meteor. Soc. Japan,* **80,** 1395–1414.

Shusse, Y., K. Tsuboki, B. Geng, H. Minda, and T. Takeda, 2005: Structure and evolution of deeply developed convective cells in a long-lived cumulonimbus cloud under a weak vertical wind-shear condition. *J. Meteor. Soc. Japan,* **83,** 351–371.

Weisman, M. L., and J. B. Klemp, 1982: The dependence of numerically simulated convective storms on vertical wind shear and buoyancy. *Mon. Wea. Rev.,* **110,** 504–520.